scientific reports

OPEN

Comparison of noninvasive pressure-volume loops derived from cardiac magnetic resonance and transthoracic echocardiography in normal subjects

Aizhan Zhankorazova[1], Zaukiya Khamitova[1], Giovanni Tonti[2], Dinara Jumadilova[1], Bauyrzhan Toktarbay[1], Nail Khissamutdinov[3] & Alessandro Salustri[1✉]

The pressure–volume (PV) loop illustrates the changing interaction between left ventricular (LV) pressure and volume throughout a cardiac cycle, and can be reconstructed noninvasively using either cardiac magnetic resonance (CMR) or transthoracic echocardiography (TTE). While reference values have been described, a direct comparison of PV loop parameters derived from CMR and TTE data within the same group of individuals has not been reported yet. In this study, we aimed to evaluate PV loop indices obtained by both techniques in a cohort of healthy volunteers. Twenty participants underwent cine-CMR and 2D-TTE examinations during the same seven-day period at the Heart Center UMC in Astana, Kazakhstan. Image datasets were post-processed with a dedicated software to derive conventional volumetric indices together with PV loop parameters: ventricular elastance (E_{es}), arterial elastance (E_a), ventriculo-arterial coupling (VAC), stroke work (SW), PV area (PVA), and work efficiency (WE). Statistical comparisons were performed with a significance threshold defined as $p < 0.05$; Bland–Altman plots assessed agreement. E_{es}, E_a, and VAC were significantly higher, while SW, PVA, and WE were significantly lower when derived from TTE compared to CMR. These findings were confirmed at the Bland-Altman analysis. Our findings suggest that values of PV loop parameters are different according to the imaging method, which may affect their translational potential. CMR and TTE are not interchangeable for PV loop evaluation, especially in the context of follow-up examinations.

Left ventricular (LV) function can be visualized by pressure-volume (PV) loops, which plot LV pressure against LV volume. These loops graphically represent the PV dynamics of the left ventricle throughout a cardiac cycle, and help characterize ventricular performance and its response to both normal and pathological conditions. PV loop analysis was pioneered by Sagawa et al.[1]. This technique involved the insertion of a miniaturized pressure transducer into the left ventricle to directly measure intraventricular pressure in real time, and at the same time the dynamic changes in ventricular blood volume were estimated using cardiac imaging modalities or conductance catheters. While this methodology yields comprehensive insights into cardiac performance, its initial application was hampered by its invasive nature, technical complexity, and associated costs. As a result, its use was primarily limited to scenarios necessitating detailed cardiac functional assessment[2]. To overcome these limitations, Chen et al. introduced a non-invasive single-beat approach using arm-cuff blood pressure and Doppler echocardiography[3]. This method was simple enough for clinical use, however it heavily depends on image quality and operator's skill.

With the development of dedicated imaging software, PV loops can be currently derived from feature-tracking CMR or speckle-tracking echocardiography, providing a reproducible non-contrast alternative[4]. This method has enabled clinical applications of the PV loop and the parameters that can be extracted from its analysis. Patients with hypertension[5,6], coronary artery disease[7,8], and heart failure[9–11] can be evaluated for

[1]School of Medicine, Nazarbayev University, Astana 010000, Kazakhstan. [2]Department of Cardiovascular Disease, University G. D'Annunzio, Chieti-Pescara, Italy. [3]Heart Center, University Medical Center, Astana 010000, Kazakhstan. ✉email: alessandro.salustri@nu.edu.kz

Parameters	CMR	TTE	p value
HR (bpm)	71 (67; 75)	70 (64; 75)	n.s.
SBP (mmHg)	117 (113; 122)	115 (110; 121)	n.s.
DBP (mmHg)	77 (73; 80)	76 (72; 79)	n.s.
LVEDV (mL)	121 (110; 129)	87 (76; 94)	<0.001
LVESV (mL)	40 (36; 44)	34 (31; 39)	<0.028
SV (mL)	81 (69; 87)	53 (43; 59)	<0.001
LVEF (%)	67 (64; 70)	60 (56; 64)	<0.001

Table 1. Hemodynamic and LV findings of the study group.
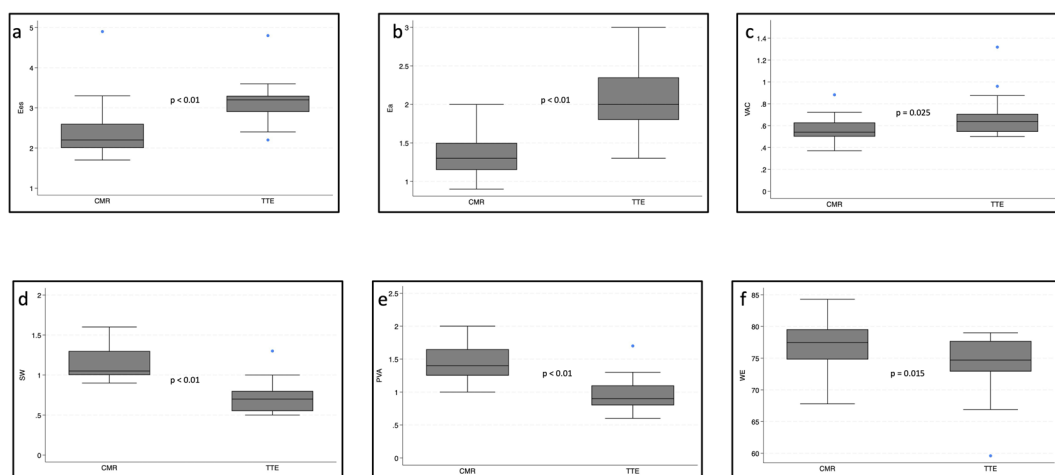
Fig. 1. Box plots of LV PV loop parameters obtained from CMR and TTE. (**a**) End-systolic elastance (E_{es}); (**b**) Arterial elastance (E_a); (**c**) Ventricular–arterial coupling (VAC); (**d**) Stroke work (SW); (**e**) Pressure–volume area (PVA); (**f**) Work efficiency (WE). Values obtained from CMR and TTE are compared for each parameter.

early detection of abnormal LV function and/or monitoring of therapeutic interventions[12–14], and our group is currently conducting such a study in the setting of hemodialysis[15]. With this approach, the information required to estimate the PV loop are extracted from the time-volume curve and the cuff brachial pressure[16,17]. Since TTE underestimates LV volumes compared to CMR[18–20], differences in PV loops and in reference values between the two imaging modalities can be anticipated. However, a comparative analysis of PV loop values within the same cohort has not yet been reported. Therefore, this study sought to compare PV loops obtained from CMR and TTE in the same cohort of healthy individuals.

Results

Table 1 outlines the main vital signs and standard LV measurements in the study group. When compared with CMR, lower LV volumes have been observed with TTE, with the most pronounced difference observed for end-diastolic volume. Accordingly, TTE-derived LVEF was slightly lower than that obtained with CMR (60% [56–64] vs. 67% [64–70]; $p < 0.001$).

The results of the PV loop analysis are represented as box plots in Fig. 1. All the parameters differed significantly when assessed by CMR and TTE. In particular, E_{es}, E_a, and VAC were significantly higher, while SW, PVA, and WE were significantly lower when derived from TTE compared to CMR. The averaged simplified CMR- and TTE-derived PV loops for the cohort of 20 volunteers are reported in Fig. 2. The figure gives a visual representation of lower SW and PVA, and steeper E_{es} and E_a by TTE compared to CMR.

The Bland–Altman plots showed good agreement of PV loop parameters between CMR and TTE measurements, with 95% of the values lying within the limits of agreement (Fig. 3). A proportional bias reached statistical significance for two parameters: E_a (slope −0.79, $p = 0.006$) and VAC (slope −0.81, $p = 0.035$). In both cases, the difference between CMR and TTE became larger as the values increased.

Correlation between the PV loop parameters and standard markers of LV function was also assessed and visualised using heatmaps, both for CMR and TTE (Fig. 4). The mean absolute correlation coefficient ($|\rho|$) across all pairs of PV loop parameters and LV function markers was calculated separately for each imaging modality. The mean $|\rho|$ was higher for TTE than for CMR (0.589 [95% CI: 0.464–0.714] vs. 0.453 [95% CI: 0.273–0.633]). However, the bootstrap comparison approach (1,000 resamples) showed that the difference between the two imaging modalities [0.136; 95% CI: 0.000–0.272] was not statistically significant ($p = 0.572$). These findings indicate that although the correlation with LV function markers looks stronger with TTE compared to CMR, the overall difference is not statistically significant. Overall, the analysis demonstrated that while systematic
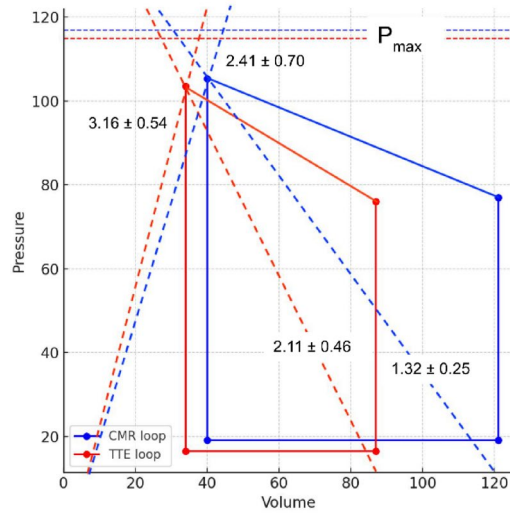
Fig. 2. Averaged simplified LV PV loops from all the 20 healthy subjects derived from CMR (blue) and TTE (red). Solid lines represent averaged PV loops; dashed lines indicate end-systolic elastances (E_{es}) and arterial elastance (E_a). Values are presented as mean ± SD.
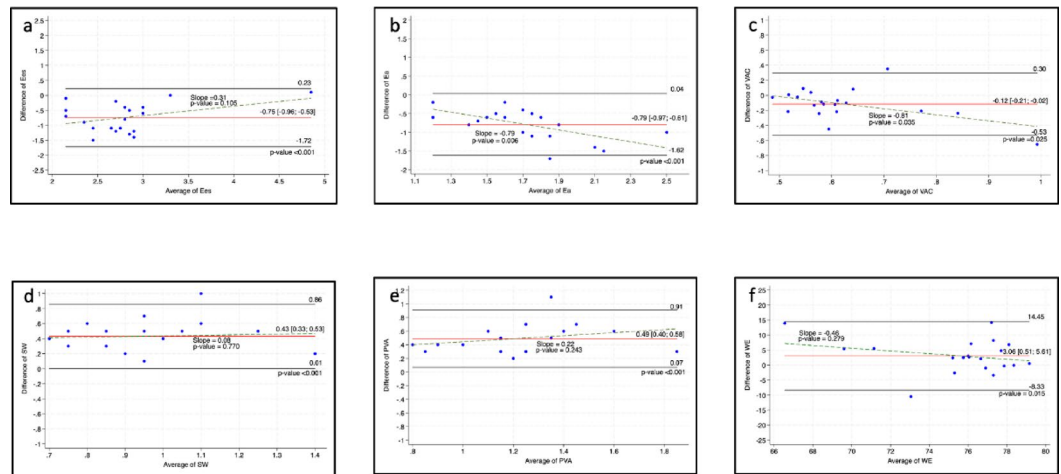

Fig. 3. Bland–Altman plots comparing PV loop parameters obtained from CMR and TTE. Each panel shows the mean difference (bias) between methods and the 95% limits of agreement: (**a**) End-systolic elastance (E_{es}); (**b**) Arterial elastance (E_a); (**c**) Ventricular–arterial coupling (VAC); (**d**) Stroke work (SW); (**e**) Pressure–volume area (PVA); (**f**) Work efficiency (WE).

differences exist between the two imaging modalities, the physiological relationships between PV loop and volumetric parameters are preserved.

Discussion

The PV loop provides a graphical representation of the LV pressure related to changes in ventricular volume throughout the cardiac cycle. It constitutes a robust quantitative tool for assessing not only the LV contractile properties but also the interaction between the left ventricle and the arterial system. Each point on the PV loop, plotted within a Cartesian coordinate framework, corresponds to a specific instantaneous PV state within the left ventricle.

Normal values of PV loop parameters have been reported for 2-D TTE[21,22]. Recently, Pedrizzetti et al. [4] have reported normal values of PV loop derived from 3D echocardiography, with several parameters stratified by sex, age, and ethnicity. When comparing data in the subgroup of subjects similar to our study group (Asian, age 18–40 years) (unpublished data provided by the authors upon request), their values fall between the values we have obtained with 2D-TTE and CMR (Table 2). This finding is not surprising, since, due to the volumetric
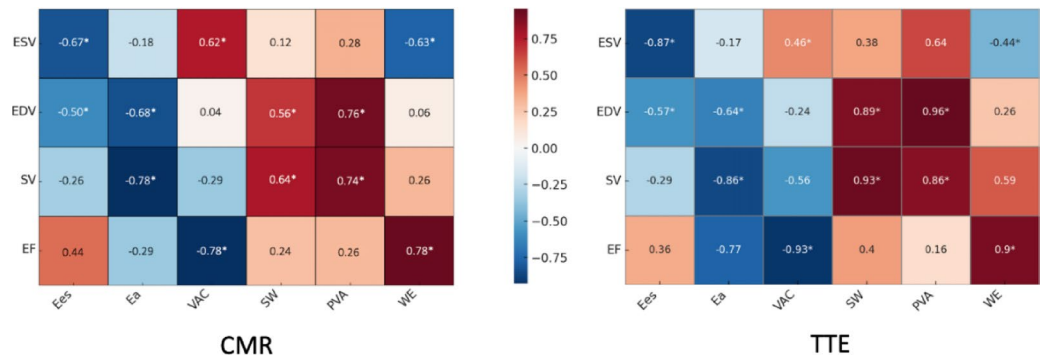
Fig. 4. Heatmaps visualization of the correlations between PV loop parameters and standard markers of LV function. Panel A: CMR-derived correlations; Panel B: TTE-derived correlations. Each cell shows the correlation coefficient ranging from − 1 (very strong negative correlation, blue) to + 1 (very strong positive correlation, red). The color gradient reflects the magnitude and direction of the correlation. Asterisks (*) indicate statistically significant correlations ($p < 0.05$). Parameters assessed include end-systolic elastance (E_{es}), arterial elastance (E_a), ventricular–arterial coupling (VAC), stroke work (SW), pressure–volume area (PVA), and work efficiency (WE) correlated against left ventricular end-diastolic volume (EDV), left ventricular end-systolic volume (ESV), stroke volume (SV), and left ventricular ejection fraction (EF).

Parameters	2D-TTE (our study)	3D-TTE [4]	CMR (our study)
Ees	3.20 (2.90; 3.30)	2.57 ± 0.60	2.20 (2.00; 2.60)
E_a	2.00 (1.80; 2.35)	1.57 ± 0.37	1.30 (1.15; 1.50)
VAC	0.64 (0.54; 0.71)	0.63 ± 0.11	0.54 (0.50; 0.63)
SW	0.70 (0.55; 0.80)	1.01 ± 0.27	1.05 (1.00; 1.30)
PVA	0.90 (0.80; 1.10)	n.a.	1.40 (1.25; 1.65)
WE	74.70 (72.9; 77.70)	75.71 ± 3.27	77.45 (74.80; 79.55)

Table 2. Left ventricular PV loop parameters obtained by 2D-TTE, 3D-TTE [4] and CMR.

approach, 3D echocardiography may overcome some limitations due to the geometric assumptions that apply to 2D echocardiography.

To date, no normative data are available for CMR-derived PV loop parameters in healthy subjects. Since PV loop reconstruction is based on LV volumes, and differences in LV volumes among different imaging modalities have been reported in previous studies[18–20], differences in PV loop according to the imaging modalities can be anticipated. However, no study has compared the values of PV loop parameters derived from CMR and TTE within the same cohort so far.

To the best of our knowledge, this is the first study to directly compare PV loop parameters derived from CMR and TTE in the same cohort of healthy adults. The results of our study indicate that, compared to CMR, TTE shows:

1. Higher values of E_{es} and E_a with a slight increase in VAC;
2. Lower SW due to the reduction in the size of PV loops;
3. Lower PVA;
4. Slight decrease in WE.

These findings are possibly related to the different LV volumes measured by CMR and TTE, which result in different shapes of the PV loop and different stroke volumes. As a consequence, the slopes of the end-systolic PV relationship (E_{es}) and of the line connecting end-diastolic volume to end-systolic PV point (E_a) are different in the PV loops derived from the two imaging modalities (see Fig. 2). Similarly, SW and PVA are underestimated by TTE due to the smaller area enclosed by the PV loop, which results in lower WE. These findings are corroborated by the assessment of the relationships between PV loop parameters and standard markers of cardiac function: overall, heatmaps analysis demonstrates that while systematic differences exist between CMR and TTE, the correlation patterns remain consistent between the two modalities, despite the differences in absolute parameter values. However, we should consider that the comparison between PV loop parameters and volumetric indices frequently yields inconsistent findings, which hamper a coherent or predictable pattern. This discrepancy occurs because the volumetric indices, conventionally employed to characterize cardiac mechanics, are largely independent of absolute pressure and insensitive to the dynamic sequence of ventricular events, thereby failing to reflect pressure-dependent determinants such as E_{es}, E_a, VAC, and myocardial energetic parameters.

Differences in PV loop morphology and PV relationships may have major diagnostic and clinical implications. In fact, the different slopes of E_{es} and E_a (both steeper with TTE compared to CMR) may suggest

a stiffened, less compliant left ventricle that must work harder to pump blood when TTE is applied as imaging modality. Moreover, due to the smaller SV, TTE underestimates LV SW when compared to CMR, which may wrongly suggest increased all-cause mortality at follow-up[23]. The observed deviations between CMR and TTE in estimating LV ESPVR and EDPVR may also have clinical implications. For instance, EDPVR has been used as a hemodynamic feature when a machine learning model was applied to predict passive myocardial properties[24]. In another study, Lav et al. demonstrated that non-invasive PV loop variables may predict the development of adverse remodelling after S-T elevation myocardial infarction[7]. Therefore, different values of PV loop parameters may affect the translational potential of the method.

Several limitations of this study must be acknowledged. Firstly, the relatively small cohort size may limit the external validity of our results. Therefore, our results should be seen as a pilot investigation rather than a definitive conclusion. Secondly, as for all imaging modalities, technological factors, including different operator experience and image quality, may impact the consistency between CMR- and TTE-derived PV loop parameters, or even among machines of the same imaging modality, leading to substantial calculation variabilities[25,26]. Thirdly, the PV loop parameters derived from TTE are inherently dependent on equipment quality, therefore the TTE-derived PV loop parameters could be different if assessed with higher-resolution echocardiographic systems. Lastly, no gold standard was defined, therefore the accuracy of each imaging modality could not be assessed. Similar to other studies comparing CMR and TTE for LV volumes and function, we might assume that PV loop parameters are more accurate when CMR is applied. Ideally, a study with a reference (invasive) method for obtaining PV loops would be desired. However, the modality-specific differences of PV loop parameters do not affect the results from previous studies on PV loops derived from CMR or TTE.

In summary, (1) reference values of PV loop parameters must be defined for each imaging modality; (2) CMR and TTE cannot be used interchangeably, particularly in follow up studies; and (3) different values of PV loop parameters may affect the translational potential of the method.

Methods

Study population

This study included the cohort of 20 healthy Kazakh adult volunteers, M/F = 13/7, median age 31 years (IQR: 27–34), already described in our recent article comparing hemodynamic forces derived from CMR and TTE[27]. All participants had both cine-CMR and 2D TTE examinations within a 7-day interval at the Heart Center, University Medical Center in Astana, Kazakhstan. Inclusion and exclusion criteria, demographic and clinical data collection, imaging protocols, and acquisition parameters for both CMR and TTE have been detailed previously[27]. For the present study, we retrospectively analyzed the same image datasets to reconstruct noninvasive PV loops.

Image acquisition

The details of the CMR protocol in our institution have been already reported[28]. In short, cine-CMR without contrast was performed using a Siemens Magnetom Avanto 1.5T scanner, following the routine cardiac sequences as advised by the European Association of Cardiovascular Imaging (EACVI)[29]. The localiser scans were acquired using True Fast Imaging with Steady-State Free Precession (TRUFI), multi 2Ch-view, Integrated Parallel Acquisition Techniques (IPAT), and four-chamber (4Ch) view. These were followed by white-blood image acquisitions in long-axis 4Ch-, 2Ch-, and 3Ch-, and short-axis views. For all acquisitions the distance factor was kept at 20% with a slice thickness of 8 mm, a repetition time (TR) of 34.68 ms, and an echo time (TE) of 1.22 ms.

TTE was obtained with a Philips Affinity 70 system using an X5-1 transducer (1–5 MHz). The examination scheme emphasized standard apical views (2-, 3-, and 4-chamber) in line with EACVI guidelines[30]. For both modalities, acquisition settings were adjusted to achieve adequate temporal (CMR: 30–50 fps; TTE: 50 fps) and spatial (CMR: 1.8×1.8 mm in-plane, 6–8 mm through-plane; TTE: axial 1.5 mm) resolution for later analysis. Blood pressure was obtained from a standard brachial cuff measurement immediately prior to image acquisition.

Image analysis

Datasets were digitally stored and analyzed offline using specialised software (Qstrain version 1.3.0.79, Medis, Leiden, the Netherlands). Source images were obtained from the institutional PACS archive in DICOM format. All datasets were anonymized prior to analysis, and the investigators were blinded to clinical data to ensure objective quantification. Two independent readers (DJ, AZ), both experienced in quantitative analysis with this software, performed the analysis.

The software reconstructs PV loops by combining the time–volume curve with brachial arterial pressure (Fig. 5). After manual selection of end-diastolic and end-systolic frames in the 2-, 3-, and 4-chamber views, the observers delineated the LV endocardial borders. A semi-automated contour detection tool was then used to assist in refining these borders. The LV outflow tract, papillary muscles, and trabeculae were considered part of the LV cavity. All contours were carefully reviewed and manually adjusted by the observers to ensure anatomical accuracy. Finally, patient-specific brachial systolic pressure was entered into the software and combined with the time–volume curve to reconstruct the PV loop. The process for obtaining a PV loop is detailed by Pedrizzetti et al.[4]. It involves generating the loop from the end-systolic PV relationship (ESPVR), the end-diastolic PV relationship (EDPVR), the coordinates identifying end-systolic volume (ESV) and end-diastolic volume (EDV), and the horizontal reference line provided by brachial systolic pressure.

PV loop parameters

The main properties of the PV loop can be described by a series of parameters. In addition to the ventricular elastance (E_{es}), the arterial elastance (E_a) is evaluated as the ratio between end-systolic pressure and stroke
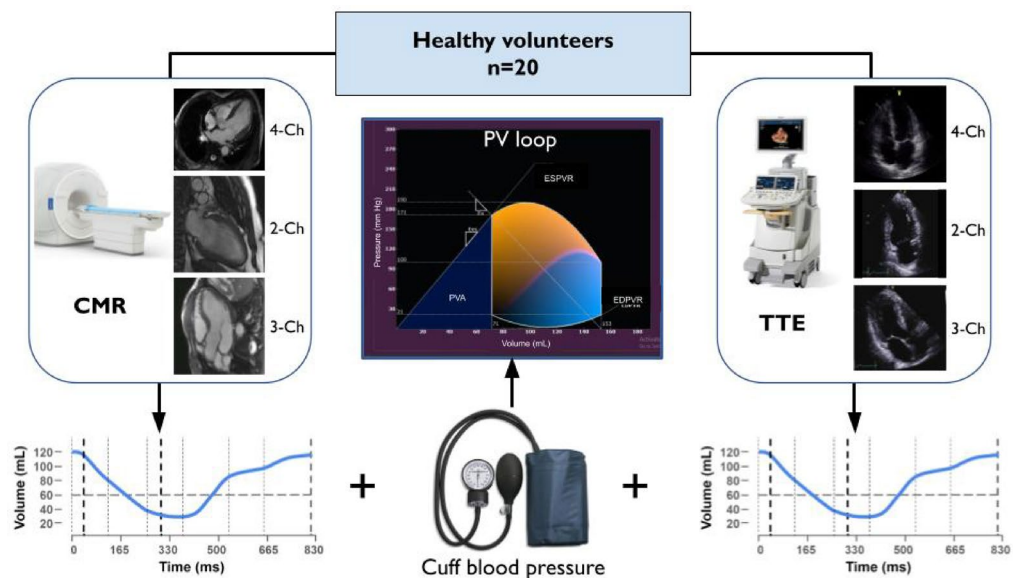
Fig. 5. Workflow for PV loop reconstruction using cardiac magnetic resonance (CMR) and transthoracic echocardiography (TTE). Left ventricular endocardial borders were manually delineated in the 4-, 2-, and 3-chamber views. Speckle-tracking analysis was used to extract volume-time curves. Please, note that we have used the same volume-time curve for both methods only for simple and easy representation of the workflow. Patient-specific brachial systolic pressure was then incorporated into the model. PV loops were generated using dedicated software that integrates imaging-derived volume curves and cuff-measured pressure to construct end-systolic and end-diastolic PV relationships.

End-systolic pressure-volume relationship (ESPVR)	The ESPVR describes the maximal pressure that the ventricle can develop at any given cardiac chamber volume. This implies that the PV loop cannot cross the line defining ESPVR for any contractile state.
End-systolic pressure (ESP)	Pressure in the ventricle at the end of systole.
End-systolic volume (ESV)	Volume of the ventricle at the end of systole.
End-diastolic pressure-volume relationship (EDPVR)	The EDPVR describes the ventricle passive filling curve and reflects the myocardium passive properties. At any point on this curve, its slope corresponds to the inverse of ventricular compliance (i.e., ventricular stiffness).
End-diastolic pressure (EDP)	Pressure in the ventricle at the end of diastole.
End-diastolic volume (EDV)	Volume of the ventricle at the end of diastole.
Ventricular elastance (E_{es})	Slope of the end-systolic pressure-volume relationship.
Arterial elastance (E_a)	Effective arterial elastance (E_a) reflects the load imposed by the arterial system on the left ventricle. Geometrically, it is illustrated by the slope of the line that joins end-diastolic volume with the end-systolic point on the PV loop. In practice, Ea is commonly estimated as the ratio of end-systolic pressure to stroke volume.
Ventriculo-arterial coupling (VAC)	VAC describes the relationship between ventricular contractility and arterial load, quantified as the ratio of arterial elastance to ventricular elastance (E_a/E_{es}). It reflects energy transfer efficiency from the heart to the arterial system. Optimal VAC balances cardiac performance and metabolic efficiency, typically around a ratio of 1.0 in healthy physiology.
Pressure-volume (PV) loop	Graph of a ventricle pressure (y-axis) and volume (x-axis) over a single cardiac cycle.
Stroke work (SW)	Ventricular stroke work refers to the amount of mechanical work generated by the left or right ventricle to eject its stroke volume into the aorta or pulmonary artery, respectively. On a PV loop, it is approximated by the area enclosed within the loop.
Potential energy (PE)	Elastic potential energy of the heart is defined by the area between the ESPVR and EDPVR curves to the left of the PV loop. $PE = ESP(ESV-V_0)/2 - EDP(EDV-V_0)/4$, where V_0 is the theoretical volume when no pressure is generated.
Pressure-volume area (PVA)	The pressure–volume area (PVA) reflects the overall mechanical energy produced during ventricular contraction. It is calculated as the sum of the stroke work (SW) represented within the PV loop and the elastic potential energy (PE) stored in the myocardium.

Table 3. Glossary of terms.

volume [$E_a = ESP/(EDV - ESV)$], and from the ratio of the two elastance values (E_a/E_{es}) the ventriculo-arterial coupling (VAC) can be calculated. The energetic properties are summarized in term of stroke work (SW), given by the area of the PV loop; the potential energy (PE), given by the area of the triangle made by the ESPVR and the PV loop, which is given by $PE = \frac{1}{2} EDP (ESV - V_0)$; the total PV area ($PVA = SW + PE$); and the work efficiency ($WE = SW/PVA$). A glossary of the main parameters is reported in Table 3.

Inter-observer reproducibility for TTE-derived VAC was evaluated in our laboratory and found to be moderate to good (E_{es}: ICC 0.88 [0.61–0.97], $p = 0.001$; E_a: ICC 0.71 [0.06–0.91], $p = 0.014$; VAC: ICC 0.67 [0.01–0.90], $p = 0.029$), and intra-observer reproducibility was good to excellent (E_{es}: ICC 0.94 [0.79–0.98], $p < 0.001$; E_a: ICC 0.97 [0.89–0.99], $p < 0.001$; VAC: ICC 0.73 [0.12–0.92], $p = 0.018$).

Statistical analysis

The Shapiro-Wilk test was used to evaluate the normality of continuous data distributions. Based on these results, paired t-tests were applied for normally distributed variables, whereas the Wilcoxon signed-rank test was used when the assumption of normality was not met. Agreement between CMR- and TTE-derived parameters was further examined with Bland–Altman analyses. Correlation analyses between PV loop parameters and other markers of LV function were performed using Spearman's or Pearson's methods as appropriate, and the results were visualized in the form of heatmaps. Each cell in the heatmap represents the correlation coefficient between a pair of variables, with values ranging from −1 (very strong negative correlation) to +1 (very strong positive correlation), and 0 indicating no association. The strength of correlation was classified as weak ($|\rho|$ <0.30), moderate ($|\rho|$ = 0.30–0.39), strong ($|\rho|$ = 0.40–0.69), or very strong ($|\rho|$ >0.70). These visualizations were used to assess modality-specific variations. To provide a quantitative summary of the overall correlation between PV loop parameters and LV function standard markers, the mean absolute correlation coefficient ($|\rho|$) was calculated across all variable pairs separately for CMR and TTE. The bootstrap comparison approach (1,000 resampling) was used to estimate 95% CI for the mean $|\rho|$ and to assess the difference in mean $|\rho|$ between imaging modalities. All statistical analyses were performed in Stata version 18.0 (StataCorp, College Station, TX), and the statistical significance level was defined as a p-value below 0.05.

Data availability

The data underlying this article will be shared on reasonable request to the corresponding author.

References

1. Sagawa, K., Suga, H., Shoukas, A. A. & Bakalar, K. M. End-systolic pressure/volume ratio: a new index of ventricular contractility. *Am. J. Cardiol.* **40**, 748–753 (1977).
2. Toktarbay, B., Zhankorazova, A., Khamitova, Z., Jumadilova, D. & Salustri, A. Ventricular-arterial coupling: advances and current perspectives in cardiovascular research. *J. Clin. Med. Kaz.* **21**, 4–10 (2024).
3. Chen, C. H. et al. Noninvasive single-beat determination of left ventricular end-systolic elastance in humans. *J. Am. Coll. Cardiol.* **38**, 2028–2034 (2001).
4. Pedrizzetti, G. et al. Noninvasive assessment of left ventricular performance using pressure–volume loops, blood propulsion and strain tensors: results from the world alliance of societies of echocardiography study. *Eur. Heart J. Cardiovasc. Imaging* (2025).
5. Lam, C. S. et al. Effect of antihypertensive therapy on ventricular-arterial mechanics, coupling, and efficiency. *Eur. Heart J.* **34**, 676–683 (2013).
6. Iakovou, I., Karpanou, E. A., Vyssoulis, G. P., Toutouzas, P. K. & Cokkinos, D. V. Assessment of arterial ventricular coupling changes in patients under therapy with various antihypertensive agents by a non-invasive echocardiographic method. *Int. J. Cardiol.* **96**, 355–360 (2004).
7. Lav, T. et al. Non-invasive pressure–volume loops provide incremental value to age, sex, and infarct size for predicting adverse cardiac remodelling after ST-elevation myocardial infarction. *Eur. Heart J. Imaging Methods Pract.* **3**, qyaf008 (2025).
8. Trambaiolo, P. et al. Evaluation of ventriculo-arterial coupling in ST elevation myocardial infarction with left ventricular dysfunction treated with Levosimendan. *Int. J. Cardiol.* **288**, 1–4 (2019).
9. Ky, B. et al. Ventricular-arterial coupling, remodeling, and prognosis in chronic heart failure. *J. Am. Coll. Cardiol.* **62**, 1165–1172. https://doi.org/10.1016/j.jacc.2013.03.085 (2013).
10. Arvidsson, P. et al. Noninvasive pressure–volume loops predict major adverse cardiac events in heart failure with reduced ejection fraction. *JACC Adv.* **3**, 100946 (2024).
11. Ikonomidis, I. et al. The role of ventricular–arterial coupling in cardiac disease and heart failure: assessment, clinical implications and therapeutic interventions. *Eur. J. Heart Fail.* **21**, 402–424 (2019).
12. Dekleva, M. et al. Improvement of ventricular-arterial coupling in elderly patients with heart failure after beta blocker therapy: results from the CIBIS-ELD trial. *Cardiovasc. Drugs Ther.* **29**, 287–294 (2015).
13. Zanon, F. et al. Ventricular-arterial coupling in patients with heart failure treated with cardiac resynchronization therapy: May we predict the long-term clinical response? *Eur. J. Echocardiogr.* **10**, 106–111 (2009).
14. Aslanger, E. et al. Effects of cardiopulmonary exercise rehabilitation on left ventricular mechanical efficiency and ventricular-arterial coupling in patients with systolic heart failure. *J. Am. Heart Assoc.* **4**, e002004 (2015).
15. Salustri, A. et al. Intradialytic changes and prognostic value of ventriculo-arterial coupling in patients with end-stage renal disease: protocol for an observational prospective trial. *JMIR Res. Protoc.* **14**, e71948 (2025).
16. Seemann, F. et al. Noninvasive quantification of pressure–volume loops from brachial pressure and cardiovascular magnetic resonance. *Circ. Cardiovasc. Imaging.* **12**, e008493 (2019).
17. Arvidsson, P. M. et al. Non-invasive left ventricular pressure–volume loops from cardiovascular magnetic resonance imaging and brachial blood pressure: validation using pressure catheter measurements. *Eur. Heart J. Imaging Methods Pract.* **1**, qyad035 (2023).
18. Bellenger, N. Comparison of left ventricular ejection fraction and volumes in heart failure by echocardiography, radionuclide ventriculography and cardiovascular magnetic resonance. Are they interchangeable? *Eur. Heart J.* **21**, 1387–1396 (2000).
19. Hoffmann, R. et al. Analysis of left ventricular volumes and function: a multicenter comparison of cardiac magnetic resonance imaging, cine ventriculography, and unenhanced and contrast-enhanced two-dimensional and three-dimensional echocardiography. *J. Am. Soc. Echocardiogr.* **27**, 292–301 (2014).
20. Gruszczyńska, K. et al. Statistical agreement of left ventricle measurements using cardiac magnetic resonance and 2D echocardiography in ischemic heart failure. *Med. Sci. Monit.* **18**, MT19–MT25 (2012).
21. Starling, M. R. Left ventricular–arterial coupling in humans. *Cardiol. Clin.* **11**, 73–87 (1993).
22. Chen, C. H. et al. Coupled systolic–ventricular and vascular stiffening with age: implications for pressure regulation and cardiac reserve in the elderly. *J. Am. Coll. Cardiol.* **32**, 1221–1227 (1998).
23. Jentzer, J. C. et al. Noninvasive echocardiographic left ventricular stroke work index predicts mortality in cardiac intensive care unit patients. *Circ. Cardiovasc. Imaging.* **13**, e011642 (2020).
24. Babaei, H. et al. A machine learning model to estimate myocardial stiffness from EDPVR. *Sci. Rep.* **12**, 5433 (2022).
25. Mukherjee, T. et al. In-silico heart model Phantom to validate cardiac strain imaging. *Comput. Biol. Med.* **181**, 109065 (2024).
26. Schmitt, B. et al. Integrated assessment of diastolic and systolic ventricular function using diagnostic cardiac magnetic resonance catheterization: validation in pigs and application in a clinical pilot study. *JACC Cardiovasc. Imaging.* **2**, 1271–1281 (2009).
27. Zhankorazova, A. et al. Comparison of left ventricular hemodynamic forces measured by transthoracic echocardiography and cardiac magnetic resonance imaging in healthy adults. *Sci. Rep.* **15**, 29796 (2025).

28. Jumadilova, D. et al. Differences in cardiac mechanics assessed by left ventricular hemodynamic forces in athletes and patients with hypertension. *Sci. Rep.* **14**, 27402 (2024).
29. Messroghli, D. R. et al. Clinical recommendations for cardiovascular magnetic resonance mapping of T1, T2, T2* and extracellular volume: a consensus statement by the society for cardiovascular magnetic resonance endorsed by the European association for cardiovascular imaging. *J. Cardiovasc. Magn. Reson.* **19**, 75 (2017).
30. Lang, R. M. et al. Recommendations for cardiac chamber quantification by echocardiography in adults: an update from the American society of echocardiography and the European association of cardiovascular imaging. *Eur. Heart J. Cardiovasc. Imaging.* **16**, 233–271 (2015).

Competing interests
The authors declare no competing interests.

Ethical approval
The investigation adhered to the Declaration of Helsinki and was reviewed and approved by the Institutional Research Ethics Committee of the Nazarbayev University (approval number: 901/13052024). Written consent was obtained from every participant prior to study enrollment. To protect confidentiality, each subject was given a study ID. Paper documents were kept in locked cabinets in the investigators' office, while electronic files were kept on computers secured with password protection. Only members of the research team directly involved in the project had access to these data.

Additional information
Correspondence and requests for materials should be addressed to A.S.

Reprints and permissions information is available at www.nature.com/reprints.

Publisher's note Springer Nature remains neutral with regard to jurisdictional claims in published maps and institutional affiliations.